Cellulose (2022) 29:117–131
https://doi.org/10.1007/s10570-021-04291-x

ORIGINAL RESEARCH

Interpreting SAXS data recorded on cellulose rich pulps

Per Tomas Larsson · Jasna Stevanic-Srndovic · Stephan V. Roth · Daniel Söderberg

Received: 27 May 2021 / Accepted: 25 October 2021 / Published online: 10 November 2021

Abstract A simulation method was developed for modelling SAXS data recorded on cellulose rich pulps. The modelling method is independent of the establishment of separate form factors and structure factors and was used to model SAXS data recorded on dense samples. An advantage of the modelling method is that it made it possible to connect experimental SAXS data to apparent average sizes of particles and cavities at different sample solid contents. Experimental SAXS data could be modelled as a superposition of a limited number of simulated intensity components and gave results in qualitative agreement with CP/MAS ^{13}C-NMR data recorded on the same samples. For the water swollen samples, results obtained by the SAXS modelling method and results obtained from CP/MAS ^{13}C-NMR measurements, agreed on the ranking of particle sizes in the different samples. The SAXS modelling method is dependent on simulations of autocorrelation functions and the time needed for simulations could be reduced by rescaling of simulated correlation functions due to their independence of the choice of step size in real space. In this way an autocorrelation function simulated for a specific sample could be used to generate SAXS intensity profiles corresponding to all length scales for that sample and used for efficient modelling of the experimental data recorded on that sample.

Supplementary Information The online version contains supplementary material available at https://doi.org/10.1007/s10570-021-04291-x.

P. T. Larsson (✉) · J. Stevanic-Srndovic
RISE Bioeconomy, Drottning Kristinas Väg 61, 114 86 Stockholm, Sweden
e-mail: tomas.larsson@ri.se

P. T. Larsson
Wallenberg Wood Science Center, KTH Royal Institute of Technology, 100 44 Stockholm, Sweden

S. V. Roth
DESY, Notkestrasse 85, 22607 Hamburg, Germany

S. V. Roth · D. Söderberg
KTH Royal Institute of Technology, 100 44 Stockholm, Sweden

Graphical abstract

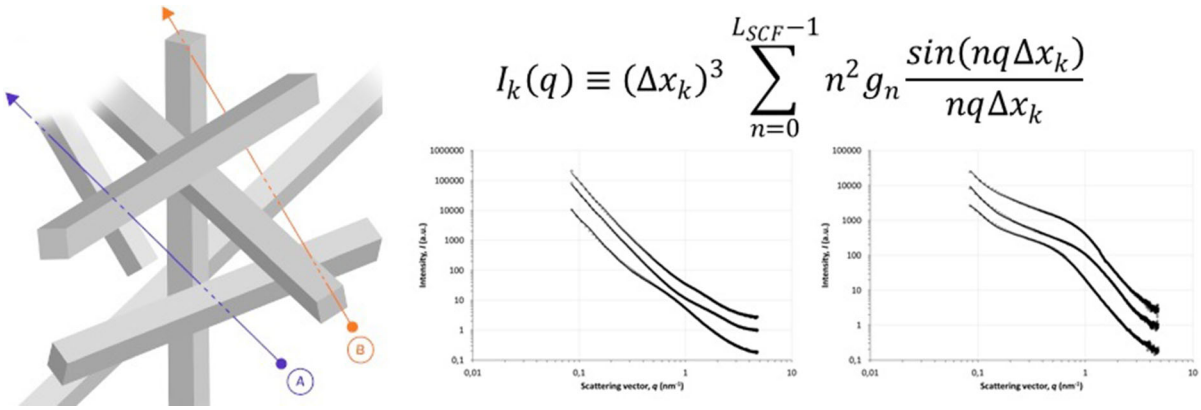

Keywords SAXS · Modelling · Cellulose · CP/MAS ^{13}C-NMR · FSP; Pulp

Background

Small Angle X-ray Scattering (SAXS) is a versatile technique that can be used to obtain quantitative measurements of the nanostructure in cellulose containing samples (Jakob et al. 1994, 1996; Fratzl 2003; Keckes et al. 2003; Penttilä et al. 2019). The character of cellulose containing samples can span a great variety (Foster et al. 2018), be it cellulose nanocrystals (CNCs), cellulose nano fibrils (CNFs) or cellulose rich pulps, which are used for the preparation of CNCs and CNFs (Foster et al. 2018). In the former case cellulose rich pulps are subjected to acid hydrolysis, normally by use of concentrated sulfuric acid, breaking down the anatomy of the pulp fibre, yielding dispersions of charged cellulose nano-particles (Elazzouzi-Hafraoui et al. 2008; Foster et al. 2018). CNFs are made by mechanical homogenization of cellulose rich pulps or chemically modified cellulose rich pulps (Pääkkö et al. 2007; Saito et al 2007). Water-based dispersions of CNCs and CNFs have been the target of some recently published studies illustrating the capacity of the SAXS technique (Håkansson et al. 2014; Su et al 2015; Phan-Xuan et al. (2016); Geng et al. 2017; Mao et al. 2017; Rosén et al. 2018; Brett et al. 2020).

Recent work points to the generation of a high aspect ratio assembly of 18 parallel β-(1 → 4)-D-glucan polymers during the biosynthesis of cellulose I (Nixon et al. 2016; Vandavasi et al. 2016; Purushotham et al. 2020; Singh et al. 2020). This would give a polymer assembly width of about 2.0 to 2.5 nm. However, in cellulose rich pulps (i.e., after pulping) experimental evidence points to polymer assemblies significantly larger than predicted by the 18-chian model (Wickholm et al. 1998; Pääkkö et al. 2007; Elazzouzi-Hafraoui et al. 2008; Fall et al. 2011; Su et al. 2015). The polymer assembly width in these cases is reported to be in the range of 4 to 5 nm. This seeming conflict can most likely be resolved if the harsh conditions during pulping are taken into consideration. During Kraft pulping, for example, wood chips are treated with high concentrations of alkali and sulfidity at temperatures in the range of 150 to 170 °C for several hours (Sixta et al. 2006). The supramolecular structure of cellulose I before and after pulping need not be the same. In this work the focus is on what we refer to as *isolated cellulose*, meaning cellulose after pulping, emphasising that it may be distinct from cellulose prior to pulping or other isolation procedures.

Wood pulps are a renewable commodity produced world-wide in large volumes for use in paper, packaging, hygiene products, and textiles. The global production of wood pulps was estimated at 144 million tonnes in 2019 (FAO 2016). Wood pulps are composed of separated anatomical plant fibres enriched in cellulose. The fibre wall of a pulp fibre contains isolated cellulose I in a complex hierarchical arrangement (Fengel and Wegener 1989), with cavities (or pores) resulting from the removal of lignin and hemicelluloses. Wood and wood pulps have been the

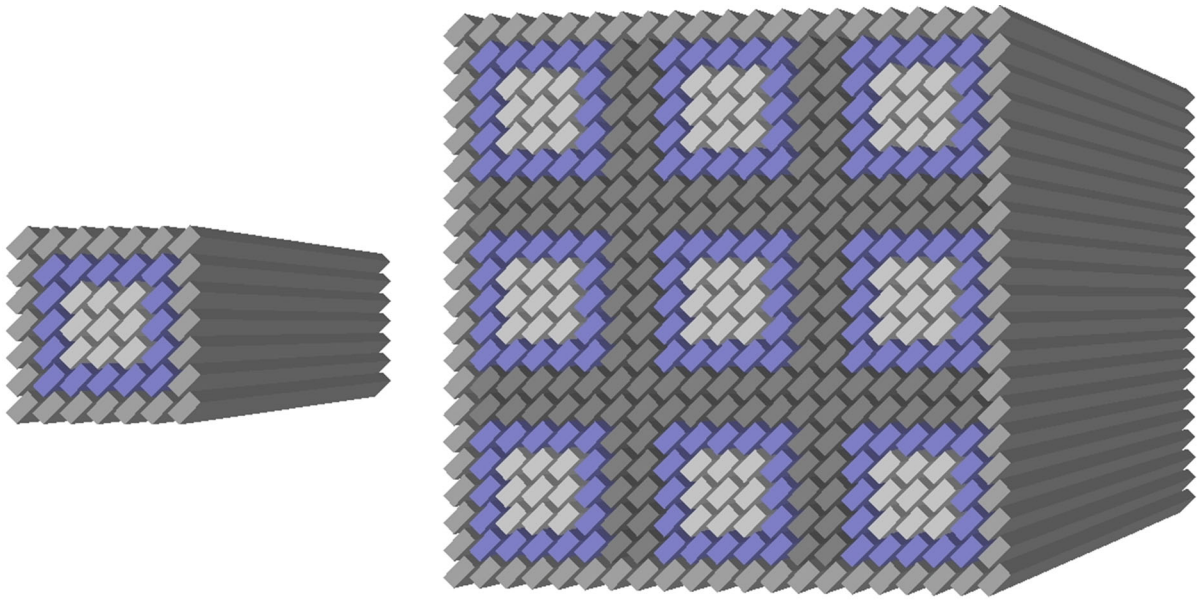

Fig. 1 A simplified and idealized representation of a longitudinal segment of a cellulose fibril composed of 7-by-7 polymers (left), and a fibril aggregate comprising 3-by-3 fibrils (right). The fibril aggregate is shown as a compact structure with no interstitial spaces between neighbouring fibrils. The depicted structures are the models used to obtain average lateral fibril and average lateral fibril aggregate dimensions based on the CP/MAS ^{13}C-NMR spectra. The ribbons represent polymers, grey: accessible surface polymers, blue: polymers in a para-crystalline form, light grey: polymers in the crystalline core, dark grey: inaccessible fibril surface polymers

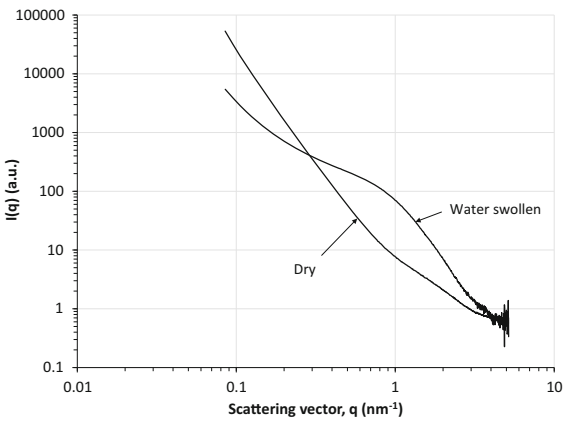

Fig. 2 Scattering intensity $I(q)$ as a function of the scattering vector q obtained from SAXS data recorded on a cellulose-rich pulp (sample HWP, see Experimental) in the water swollen and the dry state

subject of previous SAXS studies (Jakob et al. 1995; Lichtenegger et al. 1999; Fink. et al. 2004; Jungnikl et al. 2008; Virtanen et al. 2015; Mao et al. 2019).

In this work the high aspect-ratio assemblies of β-(1 → 4)-D-glucan polymers in isolated cellulose are referred to as *fibrils*. These fibrils can aggregate into larger structures, called *fibril aggregates*. The lateral and longitudinal dimensions of fibrils and fibril aggregates depend on the source material, the pulping procedure, and the drying history of a cellulose-rich pulp. Fibril aggregates combine into larger morphological features of the fibre wall, eventually forming a fibre (Fengel and Wegener 1989).

Within cellulose isolated from wood, fibrils have lateral dimensions in the range of 3 to 5 nm, and fibril aggregates can be several tens of nanometres depending on the isolation procedure and drying history of the material, Fig. 1.

Pores resulting from the removal of components during pulping can range in size from fractions of a nanometre to several tens of nanometres. Dimensionally, the widths of cellulose fibrils, cellulose fibril aggregates and pores are in the size range addressable by SAXS measurements. SAXS measurements can be performed on both dry and water swollen fibre samples, where the dry and swollen states of the same material show large structural differences, Fig. 2.

One characteristic of cellulose-rich pulps is their fibre saturation point (FSP), which describes the maximum amount of water that can be accommodated

by the pore system in the fibre wall, relative to the solids content (Stone and Scallan 1967). For cellulose rich pulps isolated from wood, the FSP has a value typically around 1 (mass of water divided by of mass solids, thus unitless). Effectively, the FSP value describes the maximum 'dilution' of the fibre wall solids that can be achieved while maintaining overall fibre structure. This is one crucial feature of cellulose rich pulps that sets it apart from CNCs and CNFs. While CNCs and CNFs samples can be prepared at high dilutions, the fibre wall that has a maximum achievable 'dilution', that is comparatively low. The fibre wall of a cellulose rich fibre is held together by strong and abundant interactions between cellulose fibrils. These interactions are strong enough to withstand the swelling pressure when in a water swollen state. In cellulose rich fibres, cellulose fibrils are arranged into a complex hierarchical fibre wall structure, with high a degree of local fibril alignment in a major part of the fibre wall (Fengel and Wegener 1989). The alignment results in strong and abundant interactions between neighbouring fibrils promoting the formation of cellulose fibril aggregates, with an associated distribution in fibril aggregate widths.

In brief, the interior of a cellulose rich fibre wall can be described as a dense network where cavity-sizes, widths, and lengths of the solid segments of the network all are associated with high degrees of variability. As a result, interpreting SAXS data from cellulose rich pulps can be a challenge. Furthermore, strong, and abundant interactions combined with large degrees of variability in the structural features makes it difficult to separate SAXS signals into contributions from form factors and structure factors (Porod 1982) even in the water swollen, most 'diluted', case.

The interior structure of a water swollen fibre wall at its saturation point (FSP) is one of the subjects of interest in this work.

In this work, an alternate strategy was attempted for the interpretation of SAXS data recorded on cellulose-rich fibres. Starting from a conceptual model representing the main features of a cellulose-rich fibre wall with abundant interactions between fibrils, SAXS intensity profiles were simulated for different particle and pore sizes. Subsequently, experimental data were modelled as a superposition of simulated SAXS intensity profiles. This way, it becomes possible to interpret the experimental SAXS data in terms of a small set of apparent average particle and apparent average pore sizes. The approach used in this work is, in some respects, like the work presented by Debye (Debye 1957). However, one advantage of the presented simulation method is that no explicit assumption of particle or cavity shape was necessary. Results from modelling of experimental data are presented and CP/MAS ^{13}C-NMR data are supplied for comparison.

Experimental

Samples

The sample materials used were pre-hydrolysed bleached softwood soda pulp (SWP), eucalyptus sulphite dissolving pulp, 96α (HWP) and cotton linters (Lint). All sample materials were initially dry. Dry samples were used after being exposed to ambient conditions for several days. Water swollen samples were placed in an excess of deionized water overnight before sample preparation and measurement.

Carbohydrate composition

Carbohydrate composition was determined according to SCAN-CM 71:09 using a high-performance anion-exchange chromatography system, Dionex ISC-5000, coupled to a CarboPac PA1 (250 mm × 4 mm i.d.) column (Dionex, Sweden) and a pulsed amperometric detector (HPAEC-PAD). The uncertainty for the relative glucose content is ± 20%.

Fibre saturation point (FSP)

Measurements were conducted in a manner similar to that of Stone and Scallan (Stone and Scallan 1967), but using only one high molecular mass dextran (Dextran 1500–2800, CAS No. 9004-54-0). Water swollen samples with a known solids content were mixed with a dextran solution of known concentration (approximately 1%, dextran mass/solution mass) in deionized water, approximately one (1) mass unit of wet sample mass being mixed with three (3) mass units of dextran solution. After mixing, the sample was stored in a sealed vessel at room temperature for three (3) days to equilibrate. A liquid sample was subsequently taken and filtered through a Puradisc syringe filter (Whatman, Maidstone, UK) equipped with a 0.45 µm polytetrafluoroethylene membrane in a polypropylene

housing (VWR International AB, Stockholm, Sweden). The concentration of dextran in the sample was determined using a calibration curve established for the optical rotation of polarized light measured using a Polartronic M100 Touch polarimeter (Schmidt + Haensch GmbH & Co., Berlin, Germany) operating at 589 nm, with a resolution of 0.001° (angular degree) and a precision of ± 0.005° at 589 nm. The calibration curve was computed using three dextran concentrations: approximately 0.5, 1.0 and 1.5% (dextran mass/solution mass), covering the range of all measurements. Dynamic light scattering was used to determine the hydrodynamic diameter of the dextran molecules at high dilution in deionized water (Zetasizer ZEN3600; Malvern Instruments Ltd., Malvern, UK), using a He–Ne 4.0 mW, 633 nm laser and a detector angle of 178°. The hydrodynamic diameter of the dextran molecules was found to be 97 ± 2 nm with a polydispersity index of 0.2, measured at a dextran concentration of 0.15 g per L solution. Based on the determined size of the dextran, the results obtained for the FSP were interpreted as representing liquid contained in pores smaller than approximately 97 nm in diameter. The FSP value is expressed as the unitless ratio of the mass of pore water to the mass of dry solids (g/g).

SAXS

X-ray measurements were performed on an Anton Paar SAXSpoint 2.0 system (Anton Paar, Graz, Austria) equipped with a Microsource x-ray source (Cu Kα radiation, wavelength 0.15418 nm) and a Dectris 2D CMOS Eiger R 1 M detector with 75 by 75 µm pixel size. All measurements were performed with a beam size of about 500 µm in diameter, at a sample stage temperature of 25 °C with a beam path pressure at 1–2 mBar. For SAXS measurements, the sample to detector distance (SDD) was 562 mm. Samples were mounted in the sample holder as shredded pulp (dry) or re-slushed pulps (water swollen). No pulp sheets were used, trying to prevent any preferential fibre orientation. Water swollen samples were mounted on a Multi-paste Holder mounted on a Heated Sampler and a VarioStage (Anton Paar, Graz, Austria). Water swollen samples were kept between Kapton foils in hermetically sealed compartments and were not exposed to vacuum during measurement. Dry samples were mounted on a Solids Sampler Holder mounted on a VarioStage (Anton Paar, Graz, Austria). The dry samples were exposed to the vacuum in the beam path. For dry sample, 6 frames each of 5 min duration were recorded, giving a total measurement time of 30 min per sample. For wet samples 10 frames of 6 min duration were recorded, giving a total measurement time of 1 h per sample. For all samples, the transmittance was determined and used for scaling of the scattering intensities. For wet samples, scattering data recorded on deionized water with the same experimental setup was used for background subtraction, an arbitrary scaling of the water signal was used. Binning was used to generate graphs with between 500 and 510 data points, which were used for graphs and modelling. The software used for instrument control was SAXSdrive version 2.01.224 (Anton Paar, Graz, Austria), and post-acquisition data processing was performed using the software SAXSanalysis version 3.00.042 (Anton Paar, Graz, Austria).

CP/MAS ^{13}C-NMR

Cross-Polarization Magic Angle Spinning Carbon-13 Nuclear Magnetic Resonance Spectra. All samples were packed uniformly in a zirconium oxide rotor. Water swollen samples had a water content of 40% to 60%. The CP/MAS ^{13}C-NMR spectra were recorded in a Bruker Avance III AQS 400 SB instrument operating at 9.4 T. All measurements were carried out at 295 (± 1) K with a magic angle spinning (MAS) rate of 10 kHz. A 4-mm double air-bearing probe was used. Data acquisition was performed using a cross-polarization (CP) pulse sequence, i.e., a 3.15 microseconds proton 90-degree pulse, 800 microseconds ramped (100–50%) falling contact pulse, with a 2.5 s delay between repetitions. A SPINAL64 pulse sequence was used for ^{1}H decoupling. The Hartmann-Hahn matching procedure was based on glycine. The chemical shift scale was calibrated to the TMS-scale (tetramethylsilane, $(CH_3)_4Si$) by assigning the data point of maximum intensity in the alpha-glycine carbonyl signal to a shift of 176.03 ppm. 4096 transients were recorded on each sample leading to an acquisition time of about 3 h. The software for spectral fitting was developed at Innventia AB and is based on a Levenberg–Marquardt algorithm (Larsson 1997). All computations were based on integrated signal intensities obtained from spectral fitting (Wickholm 1998). The errors given for parameters obtained

Table 1 Sample ID and descriptions, relative glucose contents, and fibre saturation point (FSP) of the samples used in this work

Sample ID	Description	Relative glucose content (%)	Fibre saturation point (FSP, g/g)	Volumetric fill factor (F_F, m^3/m^3)
SWP	Pre-hydrolysed bleached softwood soda pulp	97	0.40 (0.08)	0.63 (0.05)
HWP	Eucalyptus sulphite dissolving pulp, 96α	97	0.68 (0.10)	0.50 (0.04)
Lint	Cotton linters	99	0.21 (0.08)	0.76 (0.07)

Values within parenthesis are standard deviations. The volumetric fill factor (volume of solids divided by total volume) was calculated from the FSP value assuming a cellulose density of 1500 kg/m^3

Table 2 The average lateral fibril dimensions (LFD) and the average lateral fibril aggregate dimensions (LFAD) determined from CP/MAS ^{13}C-NMR spectra recorded on water swollen samples

Sample ID	LFD (nm)	LFAD (nm)
SWP	4.7 (0.1)	32 (1)
HWP	4.4 (0.1)	27 (1)
Lint	7.0 (0.2)	37 (2)

Values within parenthesis are standard errors. LFAD cannot be measured in dry samples by the used CP/MAS ^{13}C-NMR method

from the fitting procedure are the standard error with respect to the quality of the fit.

Computations

All Simulations were performed using software written in C + + utilizing parallelization. Simulations were executed on desktop PC computers, operating system Microsoft Windows® 10, running multi-core CPUs (AMD Ryzen® 7 3700X or AMD Ryzen® 9 3900X). Typical simulation times were between one to one and a half hours, depending on input parameters. Computational details are given in Supplementary Information (SI).

Results and discussions

For each sample the identity, relative glucose content, fibre saturation point (FSP) and the corresponding volumetric fill factor is given in Table 1. For the water swollen samples the FSP measurements were used to determine the volumetric fill factor, a necessary input for the simulation of relevant SAXS intensity profiles.

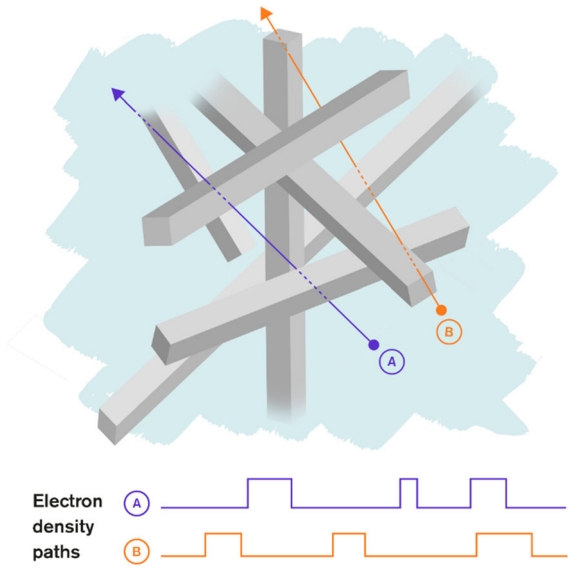

Fig. 3 A conceptual image describing how an electron density path (EDP) can be visualized in a two-component sample, here the solid material is cellulose. The EDPs shown at the bottom illustrates two examples of electron density paths encountered when following path A or path B through the sample. The grey cuboids, representing the solids, were assigned a higher electron density value, and the interstitial spaces between the grey cuboids (vacuum or water) was assigned a lower electron density value. Depending on the size-range (q-range) of modelled data the grey cuboid can represent cellulose fibrils (widths about 3–5 nm) or cellulose fibril aggregates (widths in the range of ten to several tens of nanometres). The modelling results presented in this work are based on one-dimensional electron density paths

For comparison purposes, CP/MAS ^{13}C-NMR spectra were recorded on the water swollen samples. Estimates of the average lateral fibril dimension (LFD) and the average lateral fibril aggregate dimension

(LFAD) from CP/MAS ^{13}C-NMR spectra, based on the method by Larsson and Wickholm (Larsson et al. 1997; Wickholm et al 1998) are given in Table 2.

Small angle X-ray data was recorded on dry and water swollen samples and the recorded SAXS data was modelled using a simulation model described in detail in the Supplementary Information (SI). Here only a brief account of the main features of the simulation model are given.

The simulation of SAXS intensity profiles was based on a conceptual representation of the distribution of cellulose fibrils and fibril aggregates in the fibre wall, which is illustrated in Fig. 3. The model is conceptual in the sense that it was only used as a method to design the algorithm used for generating electron density paths. One feature of this modelling strategy was that no explicit particle or cavity shape was assumed.

Once a sufficient number of electron density paths were simulated, in the order of 10^8, discrete versions of the spatial correlation function (SCF) and the pair distance distribution function (PDDF) were calculated and subsequently simulated SAXS intensity profiles, $I_k(q)$ in Equation [1], were generated. The modelling of experimental SAXS data, $I_{EXP}(q)$, was performed by superposition of simulated SAXS intensity profiles $I_k(q)$ weighted by w_k, with the addition of a modelling parameter describing any instrument background intensity b:

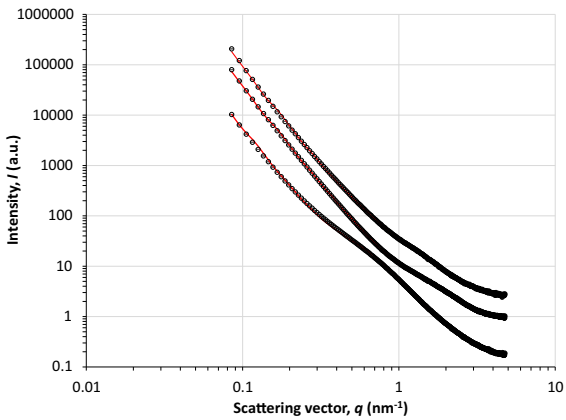

Fig. 4 Modelling results for the dry samples. Solid lines (red) represent the modelled intensity, circles represent experimental intensity. Error bars for the experimental intensity are plotted, in most cases error bars are covered by the markers. The scattering intensity has been arbitrarily scaled to minimize overlap of the curves. Top: SWP, middle: HWP, bottom Lint

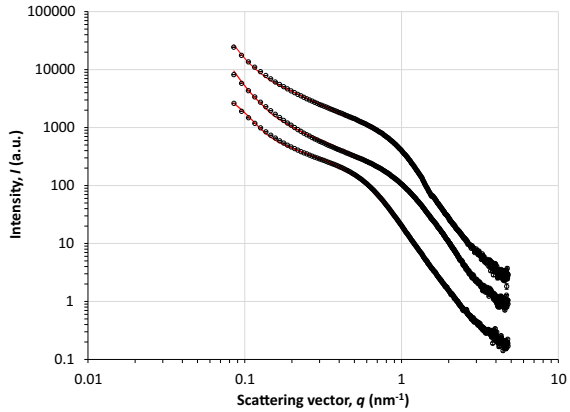

Fig. 5 Modelling results for the water swollen samples. Solid lines (red) represent the modelled intensity, circles represent experimental intensity. Error bars for the experimental intensity are plotted, in most cases error bars are covered by the markers. The scattering intensity has been arbitrarily scaled to minimize overlap of the curves. Top: SWP, middle: HWP, bottom Lint. (The kink in the SWP experimental data at a q-value about 1.5 nm^{-1} is from the detector gap.)

$$I_{EXP}(q) \approx \sum_k w_k I_k(q) + b \qquad (1)$$

The advantage of the simulation method is that it makes it possible to associate each simulated intensity profile with an apparent average particle size (AAPS) and an apparent average cavity size (AACS), connecting each intensity profile to a length scale characteristic of the structures in the sample material. Here, the concept of cavity was used to describe interstitial spaces between solid particles whether filled with water or evacuated. For all samples used in this study, three intensity components (six adjustable model parameters plus one background intensity) were used to model the experimental SAXS data.

One feature of the numerical simulation is that the generation of the SCFs is performed without any implied length scale (i.e., the generation of a SCF has no explicit x-axis). The numerically generated SCF is a real-valued vector with vector elements; SCF[0], SCF[1], …, SCF[N]. The length scale of a SCF (i.e., the length scale increment associated with a vector index increment (Δx_k)), was applied after the generation of the SCF. All simulated intensity components used for modelling experimental data from a certain sample were generated with the same volumetric fill factor, relevant to that sample. Since the generation of

Table 3 Summary of the modelling parameters used for the dry samples

	w_k (%)	Δx_k (pm)	AAPS (nm)	AACS (nm)	b	SSRR
SWP						
I_1	76 (3)	150 (10)	> 322 (110)	> 36 (12)	0.26 (0.01)	1.98
I_2	5 (1)	13 (2)	28 (10)	3.1 (1.1)		
I_3	19 (1)	4.6 (0.2)	9.9 (3.4)	1.1 (0.4)		
HWP						
I_1	78 (4)	150 (10)	> 330 (113)	> 37 (13)	0.62 (0.03)	1.00
I_2	3 (1)	17 (5)	36 (12)	4.0 (1.4)		
I_3	20 (1)	4.3 (0.1)	9.1 (3.1)	1.0 (0.3)		
Lint						
I_1	64 (2)	210 (5)	> 460 (157)	> 51 (17)	0.3 (0.02)	1.66
I_2	23 (1)	11.0 (0.2)	24 (8)	2.6 (0.9)		
I_3	14 (1)	3.7 (0.3)	7.9 (2.7)	0.9 (0.3)		

Experimental data was modelled by use of three intensity components, I_1, I_2, I_3 (Eq. 1) for all dry samples. Modelling was performed by adjusting the component weights, w_k, and the real space step size, Δx_k, for each intensity component. The "larger than" arrow in the table indicates modelling of structures too large to be unambiguously assigned using the q-range of the experimental data. The sum of squared relative residuals (SSRR) is given as an indicator of the quality of the modelling. See Supplementary Information for details

Table 4 Summary of the modelling parameters used for the water swollen samples

	w_k (%)	Δx_k (pm)	AAPS (nm)	AACS (nm)	b	SSRR
SWP						
I_1	3.9 (0.3)	100 (4)	> 72 (20)	> 42 (12)	0.16 (0.01)	4.71
I_2	5.8 (0.3)	20 (4)	14 (4)	8.4 (2.3)		
I_3	90 (6)	6.6 (0.1)	4.7 (1.3)	2.8 (0.8)		
HWP						
I_1	4.9 (0.3)	100 (10)	> 48 (13)	> 48 (13)	0.31 (0.05)	7.74
I_2	10 (1)	14.5 (0.3)	6.9 (1.8)	6.9 (1.8)		
I_3	85 (6)	5.6 (0.1)	2.7 (0.7)	2.7 (0.7)		
Lint						
I_1	5.0 (0.2)	70 (2)	> 82 (24)	> 26 (8)	0.27 (0.02)	7.77
I_2	23 (1)	14 (1)	16 (5)	5.2 (1.5)		
I_3	73 (3)	7.8 (0.2)	9.1 (2.7)	2.9 (0.9)		

Experimental data was modelled by use of three intensity components, I_1, I_2, I_3 (Eq. 1) for all water swollen samples. Modelling was performed by adjusting the component weight, w_k, and the real space step size, Δx_k, for each intensity component. The "larger than" arrow in the table indicates modelling of structures too large to be unambiguously assigned using the q-range of the experimental data. The sum of squared relative residuals (SSRR) is given as an indicator of the quality of the modelling. See Supplementary Information for details

the SCF is the most time-consuming step of the simulation, a SCF generated for a certain set of input parameters (material characteristics) can be rescaled to different length scales and subsequently used to calculate several SAXS intensity profiles in order to model experimental SAXS data recorded on a sample with those material characteristics.

Figure 4 shows the results from modelling SAXS data recorded on dry samples and Fig. 5 shows the results from modelling SAXS data recorded on the

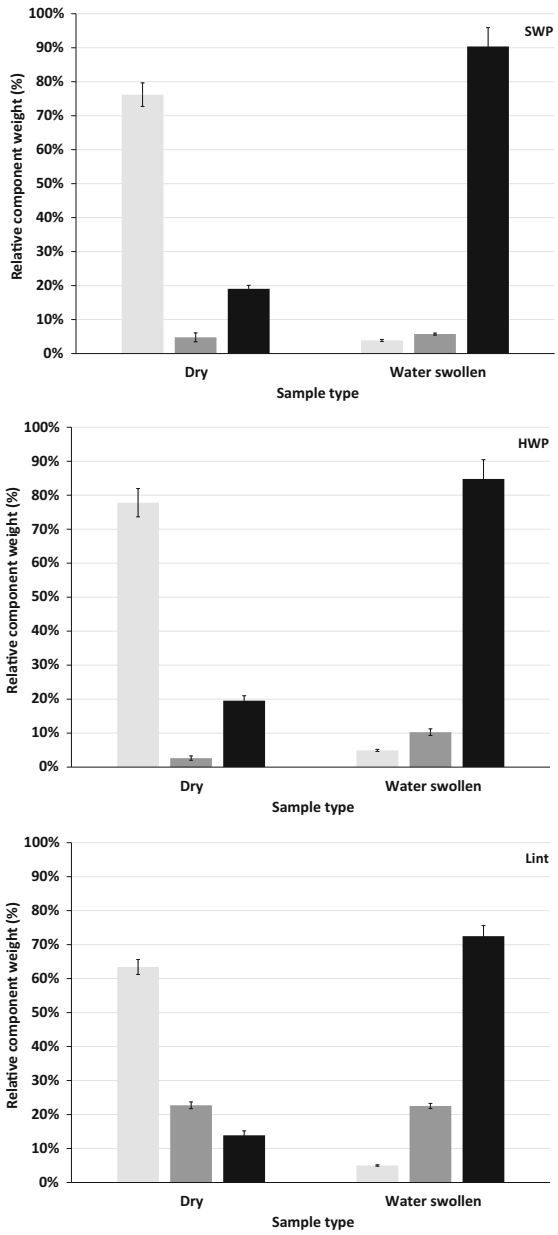

Fig. 6 The values of the relative weights for the three simulated superposition components (I_1, I_2, and I_3 in Tables 3 and 4) used to model the recorded SAXS data. From top to bottom the samples are SWP, HWP and Lint. The inset in the upper right of each panel gives the sample name. The three superposition components were viewed as representing the abundance of larger (I_1, light grey bars), intermediate (I_2, grey bars), and smaller (I_3, black bars) structural features in the samples

corresponding water swollen samples. Modelling parameters are shown in Table 3 (dry samples) and Table 4 (water swollen samples).

The values of the weights for the three simulated superposition components (I_1, I_2, and I_3 in Tables 3 and 4) used to model the recorded SAXS data are shown in Fig. 6. Although the length scales (Δx_k in Tables 3 and 4) are not identical between samples, the three superposition components are coarsely viewed as representing the abundance of larger (I_1), intermediate (I_2) and smaller (I_3) structural features in the samples.

As illustrated in Fig. 7 the presence of both cellulose fibrils and fibril aggregates forms the basis of obtaining multiple components when fitting the SAXS data. For the samples the fitting components I_2 and I_3 (Table 4) were interpreted as corresponding to the length scales between fibril aggregates and cellulose fibrils (A and F in Fig. 7), respectively. Simulating the intensity components used for modelling experimental data, the volumetric fill factor was a necessary input. For the water swollen samples the volumetric fill factor was determined from FSP measurements. For the dry samples, the volumetric fill factor cannot be determined by FSP measurements since it implies swelling of the sample, thus the volumetric fill factor was arbitrarily set to a value of 0.9, representing a dense but not a completely cavity free sample material.

In Fig. 6, the three dry samples SWP, HWP and Lint all showed large dominating structures, as modelled by the I_1 components, that gave a considerable signal intensity contribution in the observable q-range. In all the investigated dry samples the largest relative component weight (w_k) was observed for the I_1 components. This agreed with expectations, as cellulose fibrils aggregate into larger structures as a consequence of drying, contributing to hornification (Krässig 1993).

Less abundant smaller structures were observed when modelling experimental SAXS intensities of the dry samples. The AAPS corresponding to the intensity component I_2 were found to be in a size range similar to the size range of the LFAD measured by CP/MAS ^{13}C-NMR on water swollen samples, Table 2, though no direct correlation between samples was found.

The AAPS related to the intensity component I_3 showed the presence of particles larger than the LFD measured by CP/MAS ^{13}C-NMR on water swollen samples. One possible reason for this is illustrated in Fig. 8. During drying intimate local aggregation of fibrils could lead to local removal of cavities (electron

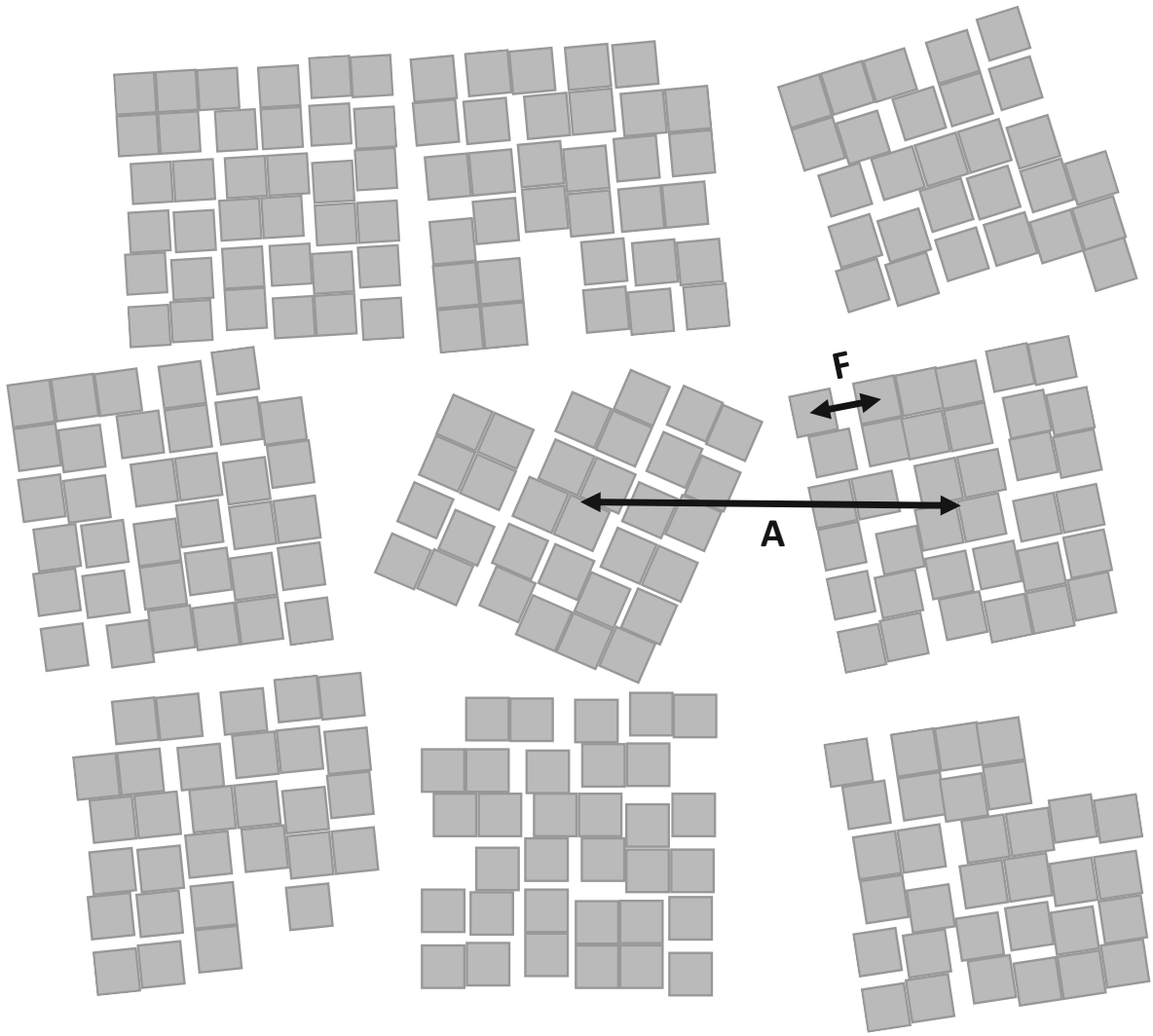

Fig. 7 An illustration of a cross-section through a part of a fibre wall showing nine fibril aggregates. The small grey squares represent the cross-sections of cellulose fibrils, with a side length of about 4 nm. Two typical length scales for electron density variations are shown. (A) shows an example of the typical distance between fibril aggregates and, (F) shows an example of the typical distance between fibrils within fibril aggregates

density contrast) between fibrils, yielding SAXS AAPS representing partial fibril aggregates. One interesting finding is that all modelling results of the SAXS data of dry samples contained an I_3 component, associated with AAPS, significantly smaller than the LFAD (CP/MAS ^{13}C-NMR, water swollen samples) and AACS values in the range of 1 nm. The I_3 component predicted by the modelling was interpreted as the existence of small-scale porosity of the cellulose structure also in the dry state, consistent with the materials known ability to rapidly re-swell. Further, the lack of correlation between the I_3 AAPS for the dry samples and LFD obtained by CP/MAS ^{13}C-NMR measurements on water swollen samples, could be explained by a larger compliance during drying of thinner fibrils. In the SWP and HWP samples, fibrils may make more intimate fibril-to-fibril contacts than the thicker, more rigid, Lint fibrils. The Lint samples showed more similar AAPS I_3-values in both the dry and the water swollen samples.

In cases where intimate proximity between fibrils reduces the electron density contrast to the point where

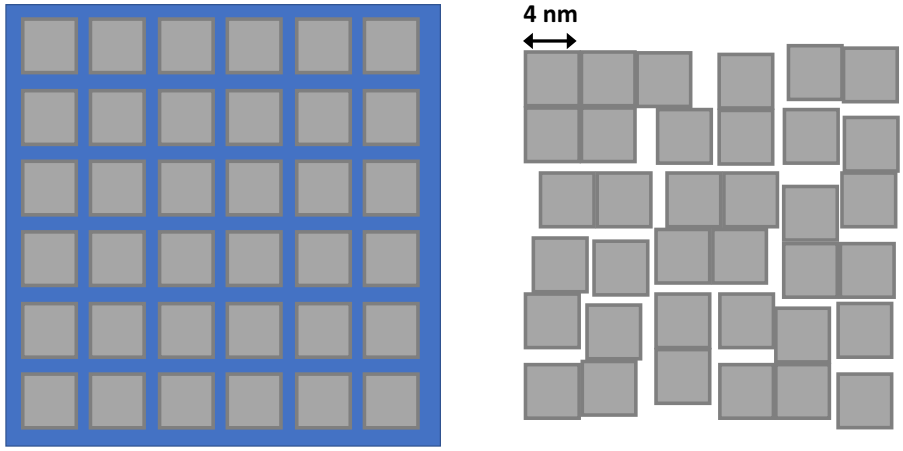

Fig. 8 An idealized illustration of a cross-section of a fibril aggregate composed of 6-by-6 fibrils, each with a width of 4 nm. Left: idealized water swollen state, right: dry state. The aggregation pattern of cellulose fibrils may vary along the length direction of a fibril aggregate. The length direction is perpendicular to the plane of the illustrated cross-section

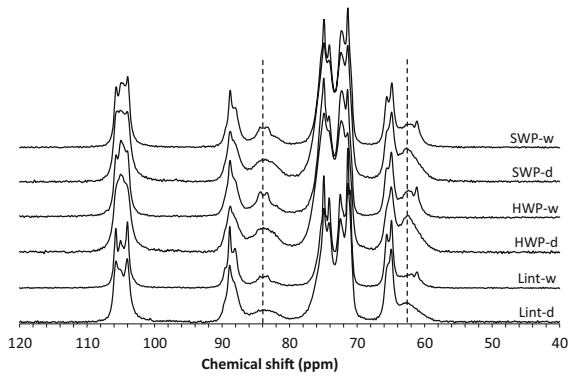

Fig. 9 CP/MAS ^{13}C-NMR spectra recorded on the samples in a dry (d) and water swollen (w) state. Signal intensity originating from fibril surface polymers is visible around 84–83 ppm (anhydroglucose C4) and 63–60 ppm (anhydroglucose C6) in both dry and water swollen samples (positions indicated by broken vertical lines). The presence of separate signals originating from fibril surface polymers in both the dry and water swollen states indicates that the conformational differences between fibril core polymers and fibril surface polymers prevails independent of the degree of compactness of the fibril aggregates

a SAXS measurement may not distinguish the width of individual fibrils, distinct fibril surface polymer conformations may still be present, allowing for CP/MAS ^{13}C-NMR to distinguish fibrils also in the dry samples. As shown in Fig. 9 the signal positions interpreted to originate from carbon-13 nuclei at the C4 and the C6 positions of the anhydroglucose units in fibril surface polymers occur at the same average positions in spectra recorded on dry and water swollen samples, though significantly broadened in the cases of dry samples.

For the water swollen samples SAXS and CP/MAS ^{13}C-NMR was used for nano-structural characterization of the cellulose rich pulp samples. The differences in the principles of operation of SAXS and CP/MAS ^{13}C-NMR opens for a possibility to obtain complementary information when applying the two techniques to the same sample. Specifically, that the modelled I_3 components, interpreted to be related to size of lateral fibrils dimensions, is related to the LFD obtained from CP/MAS ^{13}C-NMR. Similarly, the I_2 components in the water swollen samples is interpreted to be related to the lateral aggregate dimensions and thus related to lateral fibril aggregates dimensions (LFAD) obtained from CP/MAS ^{13}C-NMR.

Common to all water swollen samples is an increased abundance of smaller structural features as a consequence of swelling, compared with their dry counterparts (Fig. 6.). This agrees with expectations in that swelling increases the specific surface area and increases the abundance and size of cavities in cellulose rich fibres. This is accompanied by an increased electron density contrast at smaller length scales. In the case of water swollen samples, SAXS modelling results showed a significant reduction of the intensities originating from the I_1 component, compared with their dried counterparts (Fig. 6 and Tables 3 and 4). For intensity components I_2 and I_3 in Table 4,

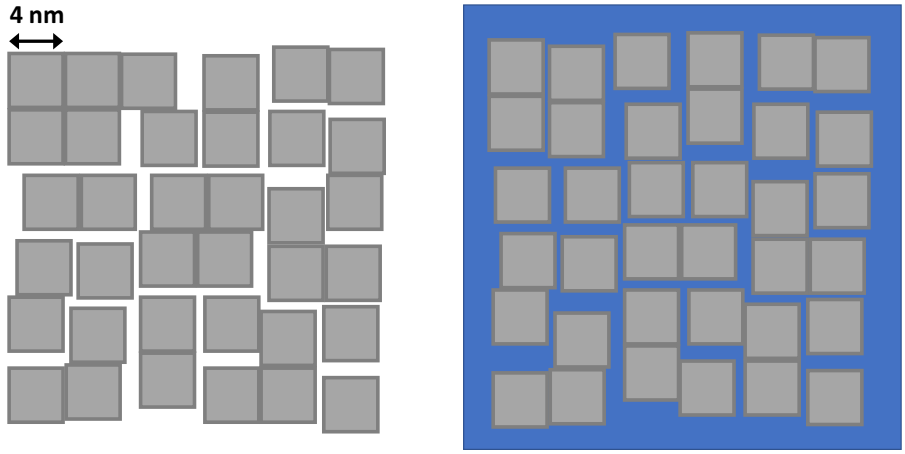

Fig. 10 An idealized illustration of the cross-section of a fibril aggregate composed of 6-by-6 fibrils, each with a width of 4 nm. Left: dry state with remaining imperfect packing of cellulose fibrils, right: water swollen state with imperfections in the cellulose fibril packing remaining. The aggregation pattern of cellulose fibrils may vary along the length direction of a fibril aggregate. The length direction is perpendicular to the plane of the illustrated cross-section

the ranking of the samples' AAPS was in the order Lint > SWP > HWP, in agreement with the sample ranking based on the CP/MAS ^{13}C-NMR LFD and LFAD measured on water swollen samples (Table 2). Consistently, the average apparent cavity size, AACS, was found to be larger for the modelled I_2 and I_3 components in the water swollen samples, compared with their dry counterparts.

For the water swollen samples, modelling of SAXS results showed that the AAPS for the I_2 intensity components (Table 4) was consistently smaller than the corresponding CP/MAS 13C-NMR LFAD measurements (Table 2). One interpretation of this observation is that the SAXS measurements can detect cavities within cellulose fibril aggregate, cavities that the CP/MAS ^{13}C-NMR measurements could not distinguish. Some support for this interpretation can be found in previous results obtained by NMR relaxometry data (Larsson 2017). Specifically, probing the cellulose specific surface area (particle surface-to-volume ratio) by ^{2}H-relaxation measurements showed results between the high limit (all fibril surfaces exposed by swelling) and the low limit of specific surface area (only fibril aggregate surfaces exposed by swelling) obtainable from CP/MAS ^{13}C-NMR measurements. This is consistent with the hornification behaviour of cellulose if part of the structures illustrated in the right-hand panel of Fig. 8 remain after re-swelling in water, resulting in a non-compact structure inside fibril aggregates (Fig. 10).

The SWP and HWP samples were produced by two different isolation procedures. The SWP was produced by an alkaline pulping process, while the HWP was produced by a comparatively more acidic pulping process. This may be an explanation for the differences observed in the SAXS modelling results for the two samples.

Conclusions

A method was developed for modelling SAXS data recorded on dense two-component systems with abundant interactions and was independent of the establishment of form factors and structure factors. Experimental SAXS data, from cellulose rich pulps, could be modelled using a limited number of simulated intensity components, and gave results, including apparent average particle sizes (AAPS), in qualitative agreement with CP/MAS ^{13}C-NMR data recorded on the same samples. In the case of water swollen samples, SAXS modelling results and NMR data agreed on the ranking of particle sizes. The time necessary for simulations could be reduced by the rescaling of simulated autocorrelation functions, due to their independence of the choice of real space step size. In this way a single autocorrelation function simulated for a specific sample could be used to generate SAXS intensity profiles corresponding to all

length scales for that sample and used for efficient modelling of experimental data.

Acknowledgments PT Larsson gratefully acknowledges 'Stiftelsen Nils och Dorthi Troëdssons forskningsfond' for funding this project by granting the application 943/18, Development of interpretation models for Small Angle X-ray Scattering measurements of cellulose materials.

Authors' contributions P.T.L.: Idea, application for funding, planning of work, sample selection and supply, programming, and program development, performing numerical simulations, writing manuscript. J.S.-S.: experimental work, FSP, scattering and CP/MAS^{13}C-NMR measurements and post-acquisition processing of data. S.R.: Scientific discussions during theoretical development and discussions of simulation results, input on manuscript. D.S.: Scientific discussions during theoretical development and discussions of simulation results, input on manuscript.

Funding Open access funding provided by RISE Research Institutes of Sweden. 'Stiftelsen Nils och Dorthi Troëdssons forskningsfond' are gratefully acknowledged for funding; application 943/18, Development of interpretation models for Small Angle x-ray Scattering measurements of cellulose materials.

Availability of data and material Can be supplied by corresponding author on request.

Code availability Can be supplied corresponding author on request.

Declarations

Conflict of interest The authors declare that they have no conflict of interest.

Consent to participate All authors of this manuscript have participated in the work willingly.

Consent for publication All authors of this manuscript give their consent to publish the presented manuscript.

References

Brett CJ, Montani S, Schwartzkopf M, van Benthem RATM, Jansen JFGA, Griffini G, Roth SV, Johansson MK (2020) Revealing structural evolution occurring from photo-initiated polymer network formation. Commun Chem 3(1):1–7. https://doi.org/10.1038/s42004-020-0335-9

Debye P, Anderson HR, Brumberger H (1957) Scattering by an inhomogeneous solid II. The correlation function and its application. J Appl Phys 28:679–683. https://doi.org/10.1063/1.1722830

Elazzouzi-Hafraoui S, Nishiyama Y, Putaux J, Heux L, Dubreuil F, Rochas C (2008) The shape and size distribution of crystalline nanoparticles prepared by acid hydrolysis of native cellulose. Biomacromol 9:57–65. https://doi.org/10.1021/bm700769

Fall AB, Lindström SB, Sundman O, Ödberg L, Wågberg L (2011) Colloidal stability of aqueous nanofibrillated cellulose dispersions. Langmuir 27(18):11332–11338. https://doi.org/10.1021/la201947x

FAO, Food and Agriculture Organization of The United Nations (2016), pulp and paper capacities, survey 2015–2020, Rome, Italy. Spread sheets with data is available at URL:http://www.fao.org/forestry/statistics/80571/en/.

Fengel D, Wegener G (1989). Chapters 2 and chapter 4 in Wood. Chemistry, Ultrastructure, Reactions. Walter de Gruyter, Berlin. https://doi.org/10.1515/9783110839654.

Fink HP, Weigel P, Ganster J, Rihm R, Puls J, Sixta H, Parajo JC (2004) Evaluation of new organosolv dissolving pulps. Part II: structure and NMMO processability of the pulps. Cellulose 11(1):85–98. https://doi.org/10.1023/B:CELL.0000014779.93590.a0

Foster EJ, Moon RJ, Agarwal UP, Bortner MJ, Bras J, Camarero-Espinosa S, Chan KJ, Clift MJD, Cranston ED, Eichhorn SJ, Fox DM, Hamad WY, Heux L, Jean B, Korey M, Nieh W, Ong KJ, Reid MS, Renneckar S, Roberts R, Shatkin JA, Simonsen J, Stinson-Bagby K, Wanasekaraq N, Youngblood J (2018) Current characterization methods for cellulose nanomaterials. Chem Soc Rev 47(8):2609–2679. https://doi.org/10.1039/c6cs00895j

Fratzl P (2003) Small-angle scattering in materials science-a short review of applications in alloys, ceramics, and composite materials. J Appl Crystallogr 36(3):397–404. https://doi.org/10.1107/S0021889803000335

Geng L, Peng X, Zhan C, Naderi A, Sharma PR, Mao Y, Hsiao BS (2017) Structure characterization of cellulose nanofiber hydrogel as functions of concentration and ionic strength. Cellulose 24(12):5417–5429. https://doi.org/10.1007/s10570-017-1496-2

Håkansson KM, Fall AB, Lundell F, Yu S, Krywka C, Roth SV, Santoro G, Kvick M, Prahl Wittberg L, Wågberg L, Söderberg LD (2014) Hydrodynamic alignment and assembly of nanofibrils resulting in strong cellulose filaments. Nat Commun 5(1):1–10. https://doi.org/10.1038/ncomms5018

Jakob HF, Fratzl P, Tschegg SE (1994) Size and arrangement of elementary cellulose fibrils in wood cells: a small-angle X-ray scattering study of Picea Abies. J Struct Biol 113(1):13–22. https://doi.org/10.1006/jsbi.1994.1028

Jakob HF, Fengel D, Tschegg SE, Fratzl P (1995) The elementary cellulose fibril in Picea Abies: comparison of transmission electron microscopy, small-angle x-ray scattering, and wide-angle x-ray scattering results. Macromolecules 28(26):8782–8787. https://doi.org/10.1021/ma00130a010

Jakob HF, Tschegg SE, Fratzl P (1996) Hydration dependence of the wood-cell wall structure in Picea Abies. A small-angle x-ray scattering study. Macromolecules 29(26):8435–8440. https://doi.org/10.1021/ma9605661

Jungnikl K, Paris O, Fratzl P, Burgert I (2008) The implication of chemical extraction treatments on the cell wall nanostructure of softwood. Cellulose 15(3):407. https://doi.org/10.1007/s10570-007-9181-5

Keckes J, Burgert I, Frühmann K, Müller M, Kölln K, Hamilton M, Burghammer M, Roth SV, Stanzl-Tschegg S, Fratzl P (2003) Cell-wall recovery after irreversible deformation of wood. Nat Mater 2(12):810–813. https://doi.org/10.1038/nmat1019

Krässig HA (1993). Chapter 2 in Cellulose. Structure, Accessibility and Reactivity, Polymer Monographs Volume 11, Gordon and Breach Science Publishers, Amsterdam. https://doi.org/10.1002/pi.1995.210360114.

Larsson PT, Wickholm K, Iversen T (1997) A CP/MAS ^{13}C-NMR investigation of molecular ordering in celluloses. Carbohyd Res 302:19–25. https://doi.org/10.1016/S0008-6215(97)00130-4

Larsson PT, Karlsson RMP, Westlund PO, Wågberg L (2017). The internal structure of isolated cellulose I fibril aggregates in the water swollen state. ACS Symposium Series book: Nanocelluloses: Their Preparation, Properties, and Applications, Editor(s): Umesh P. Agarwal, Rajai H. Atalla, and Akira Isogai, Volume 1251, Chapter 5, pp 91–112. https://doi.org/10.1021/bk-2017-1251.ch005.

Lichtenegger H, Müller M, Paris O, Riekel C, Fratzl P (1999) Imaging of the helical arrangement of cellulose fibrils in wood by synchrotron x-ray microdiffraction. J Appl Crystallogr 32(6):1127–1133. https://doi.org/10.1107/S0021889899010961

Mao J, Heck B, Abushammala H, Reiter G, Laborie MP (2019) A structural fibrillation parameter from small angle x-ray scattering to quantify pulp refining. Cellulose 26(7):4265–4277. https://doi.org/10.1007/s10570-019-02386-0

Mao Y, Liu K, Zhan C, Geng L, Chu B, Hsiao BS (2017) Characterization of nanocellulose using small-angle neutron, x-ray, and dynamic light scattering techniques. J Phys Chem B 121(6):1340–1351. https://doi.org/10.1021/acs.jpcb.6b11425

Nixon BT, Mansouri K, Singh A, Du J, Davis JK, Lee JG, Slabaugh E, Vandavasi VG, O'Neill H, Roberts EM, Roberts AW, Yingling YG, Haigler CH (2016) Comparative structural and computational analysis supports eighteen cellulose synthases in the plant cellulose synthesis complex. Sci Rep 6(1):1–14. https://doi.org/10.1038/srep28696

Penttilä PA, Rautkari L, Österberg M, Schweins R (2019) Small-angle scattering model for efficient characterization of wood nanostructure and moisture behaviour. J Appl Crystallogr 52(2):369–377. https://doi.org/10.1107/S1600576719002012

Phan-Xuan T, Thuresson A, Skepö M, Labrador A, Bordes R, Matic A (2016) Aggregation behavior of aqueous cellulose nanocrystals: the effect of inorganic salts. Cellulose 23(6):3653–3663. https://doi.org/10.1007/s10570-016-1080-1

Porod G (1982) Chapter 2, General Theory, Small angle x-ray scattering, Glatter O and Kratky O (ed.) Academic Press, London, pp 17–52.

Purushotham P, Ho R, Zimmer J (2020) Architecture of a catalytically active homotrimeric plant cellulose synthase complex. Science 369(6507):1089–1094. https://doi.org/10.1126/science.abb2978

Pääkkö M, Ankerfors M, Kosonen H, Nykänen A, Ahola S, Österberg M, Ruokolainen J, Laine J, Larsson PT, Ikkala O, Lindström T (2007) Enzymatic hydrolysis combined with mechanical shearing and high-pressure homogenization for nanoscale cellulose fibrils and strong gels. Biomacromol 8(6):1934–1941. https://doi.org/10.1021/bm061215p

Rosén T, Brouzet C, Roth SV, Lundell F, Söderberg LD (2018) Three-dimensional orientation of nanofibrils in axially symmetric systems using small-angle x-ray scattering. J Phys Chem C 122(12):6889–6899. https://doi.org/10.1021/acs.jpcc.7b11105

Saito T, Kimura S, Nishiyama Y, Isogai A (2007) Cellulose nanofibers prepared by TEMPO-mediated oxidation of native cellulose. Biomacromol 8(8):2485–2491. https://doi.org/10.1021/bm0703970

Singh A, Kwansa AL, Kim HS, Williams JT, Yang H, Li NK, Kubicki JD, Roberts AW, Haigler CH, Yingling YG (2020) In silico structure prediction of full-length cotton cellulose synthase protein (GhCESA1) and its hierarchical complexes. Cellulose 27(10):5597–5616. https://doi.org/10.1007/s10570-020-03194-7

Sixta H, Potthast A, Krotschek AW (2006) Sections 4.1–4.2.5, Chemical Pulping Processe, Handbook of pulp. In: Sixta H (ed.), Wiley-VCH Verlag GmbH & Co. KGaA, pp 109–229. https://doi.org/10.1002/9783527619887

Stone JE, Scallan AM (1967) The effect of component removal upon the porous structure of the cell wall of wood II. Swelling in water and the fibre saturation point. Tappi 50(10):496–501

Su Y, Burger C, Ma H, Chu B, Hsiao BS (2015) Exploring the nature of cellulose microfibrils. Biomacromol 16(4):1201–1209. https://doi.org/10.1021/bm501897z

Vandavasi VG, Putnam DK, Zhang Q, Petridis L, Heller WT, Nixon BT, Haigler CH, Kalluri U, Coates L, Langan P, Smith JC, Meiler J, O'Neil H (2016) A structural study of CESA1 catalytic domain of Arabidopsis cellulose synthesis complex: evidence for CESA trimers. Plant Physiol 170(1):123–135. https://doi.org/10.1104/pp.15.01356

Virtanen T, Penttilä PA, Maloney TC, Grönqvist S, Kamppuri T, Vehviläinen M, Serimaa R, Maunu SL (2015) Impact of mechanical and enzymatic pretreatments on softwood pulp fiber wall structure studied with NMR spectroscopy and x-ray scattering. Cellulose 22(3):1565–1576. https://doi.org/10.1007/s10570-015-0619-x

Wickholm K, Larsson PT, Iversen T (1998) Assignment of non-crystalline forms in cellulose I by CP/MAS ^{13}C-NMR spectroscopy. Carbohyd Res 312:123–129. https://doi.org/10.1016/S0008-6215(98)00236-5